

Finite element implementation of a glass tempering model in three dimensions

J.H. Nielsen ^{*}, J.F. Olesen, P.N. Poulsen, H. Stang

Department of Civil Engineering, Technical University of Denmark, Bovej Building 118, DK-2800 Kgs. Lyngby, Denmark

ARTICLE INFO

Article history:

Received 21 January 2010

Accepted 21 May 2010

Available online 19 June 2010

Keywords:

Residual stresses

Toughened glass

Structural relaxation

Thermorheological simple material

Strength of tempered glass

Soda-lime-silica glass

ABSTRACT

The present paper develops and validates a 3D model for the simulation of glass tempering. It is assembled from well-known models of temperature dependent viscoelasticity and structural relaxation and predicts both transient and steady-state stresses in complex 3D glass geometries. The theory and implementation of the model is comprehensively given and the model is carefully checked and validated. It is demonstrated that by adjusting a single parameter in the model, experimental results can be replicated accurately even for cooling rates far from normal.

© 2010 Elsevier Ltd. All rights reserved.

1. Introduction

1.1. Motivation

Over the last couple of decades, glass¹ has gained an increasing popularity as a structural, load carrying material due to its transparency and high resistance to environmental loadings. However, glass lacks the capability of yielding and is extremely brittle. This indicates that the tensile strength is governed by small flaws in the surface which reduce the strength of ordinary float glass to approximately 50 MPa and give rise to huge variations in the strength value.

By imposing a compressive residual stress at the surface balanced with an internal tensile stress as shown in Fig. 1, the surface flaws will be in a permanent state of compression which has to be exceeded by external loading before failure can occur. The tensile residual stresses are carried by the interior part of the material, which is (almost) flawless [3]. Such a distribution of the residual stresses can be obtained by the so-called tempering process of the glass. Glass with such a stress state is often referred to as tempered glass or toughened glass.² The strength of tempered glass is considerably higher than what is found for ordinary float glass and furthermore, the strength is more reliable and (almost) time independent [3]. However, if the residual stress state is disturbed sufficiently, the tempered glass will fragmentize completely. The fragmentation process is experimentally investigated further in [1].

When a hot glass specimen is cooled rapidly (quenched) from temperatures above the glass transition temperature, residual stresses are developed. This process is referred to as the tempering process and increases the apparent strength of the glass considerably by introducing compressive residual stresses at the surface. However, the cooling rates in such a specimen will be spatially dependent indicating that spatial variations in the residual stresses will be present. This means that the apparent strength of a tempered glass specimen is spatially dependent as indicated in (1)

$$f_t^{app}(x_i) = f_t^{mat}(x_i) - \sigma_{rs}(x_i) + f_t^{other}(x_i) \quad (1)$$

where f_t^{app} is the apparent tensile strength, x_i are the spatial Cartesian coordinates with i ranging from 1 to 3, f_t^{mat} is the inherent material strength, σ_{rs} is the residual stress (compression is negative) and f_t^{other} is a contribution to the strength originating from secondary phenomena such as crack healing during tempering. The inherent material strength, f_t^{mat} , is time dependent due to static fatigue [2] and the contribution from crack healing is relatively small. It is therefore common practice to assume the strength equal to the residual stress when designing with tempered glass [3]. Today, a simple destructive test is used for identifying the glass as tempered or not [4], however, this test does not reveal anything about local variations of the residual stresses near corners, edges and holes. Another technique is more advanced and measures the residual stresses, however, this technique cannot be used close to corners, edges and holes, where the largest loads are often applied. A numerical tool for predicting the residual stresses in tempered glass will be valuable for optimizing the tempering process as well as an important tool when designing structures in tempered glass.

* Corresponding author.

E-mail addresses: jhn@byg.dtu.dk (J.H. Nielsen), jfo@byg.dtu.dk (J.F. Olesen), pnp@byg.dtu.dk (P.N. Poulsen), hs@byg.dtu.dk (H. Stang).

¹ In this paper, only soda-lime-silica glass is considered.

² The stress state should be above a certain level before these names are used.

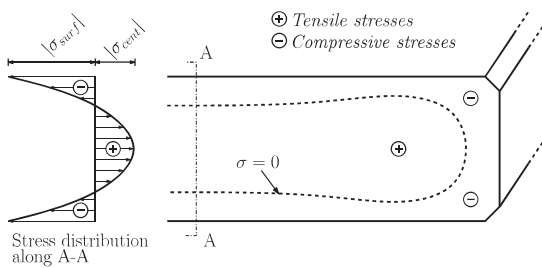


Fig. 1. Residual stresses in tempered glass. The right drawing shows a line representing the location where the residual stresses equals zero near an edge. The left drawing shows the stress distribution far from any edges (cut A-A).

In commercially tempered glass, the residual compressive stresses at the surface are often in the order of magnitude of 100 MPa. However, the residual stresses are governed by the cooling rate, but unfortunately a brutal quenching of the glass will induce high transient tensile stresses which may lead to breakage of the glass during the process. A model capable of predicting the transient residual stresses is therefore a valuable tool for the manufacturer of tempered glass in order to optimize their product.

The present paper starts by describing the foundation for constructing a model capable of predicting the tempering process in a full 3D domain. The foundation is based on well-known models, however, after the basis is formed a thorough description of how to combine and implement the models is given. The model is verified by comparison with experimental data and several examples of the use is given.

1.2. Evolution of tempering models

According to [5] the tempering process of glass was patented in 1877, however, it was not until 1920 that the first simple models were developed. Adams and Williamson [6] formulated a simple theory for the generation of residual stresses, stating that *the strain remaining in a block of glass is equal and opposite in sign to the reverse strain lost by viscous yielding in the early stages of the cooling process*. The reverse strain is to be interpreted as the strain originating from the transient temperature gradient during cooling.

In 1948, Bartenev [7] utilized that the viscosity of molten glass increases very rapidly during cooling. By assuming the glass to be a fluid, without any capability to carry stresses for temperatures above the glass transition temperature, T_g , and a linear elastic solid below T_g . This is the basic concept of the so-called instant freeze theory. The next step was to include the relaxation of stresses during the glass transition temperature range. Experimental data was provided in several papers around 1950 and 1960, showing that the relaxation of glass at different temperatures can be treated in a simple manner, see e.g. [8]. It was shown that the relaxation curves for glass at different temperatures can be brought to coincide simply by changing the timescale; a material with such behavior is said to be thermorheologically simple (TS) [9]. In 1965, Lee, Rogers and Woo [10] introduced a model including the TS behavior of glass.

The most recent step in developing the theory for the tempering process was to include the so-called structural relaxation, which accounts for the fact that the slower a glass is cooled the more regular the long range order becomes which affects certain properties. A model for such behavior was proposed by Narayanaswamy [11] using the concept of fictive temperatures introduced by Tool in 1946 [12]. It was found that the volume change was by far the property that contributed the most to the residual stresses [13], and often the theory is referred to as volume relaxation. At the time of development, only the in-plane stress distribution through

the thickness of a plate far from any edges was considered, i.e. the one-dimensional case, however, modern computers provide enough computational power for analyzing complex geometries in three dimensions.

Although, a theory for the tempering process is available, the application to engineering practice seems remote at the present time. However, it is the view of the authors, that this remoteness is caused by a lack of knowledge regarding the theory and its implementation using numerical methods.

Implementations of tempering models have been reported recently, see e.g. [14] or [15]. However, the focus of these papers is on particular results without a detailed description of the algorithm nor an extensive verification of the model is given.

The present paper provides the reader with the theory of the constitutive behavior of glass during quenching and provides detailed information on how to implement a full 3D algorithm in a finite element program. Furthermore, a verification and a finite element convergency analysis of the implementation is performed.

2. Theory

This section presents the basis for a tempering model capable of predicting both transient and steady-state residual stresses in tempered glass. The tempering model is formed by three main ingredients, namely temperature dependent viscoelasticity, structural volume relaxation and the temperature history. Only the two first will be considered in detail, the temperature history is assumed known. For the examples given, the temperature problem is solved using a simple convective boundary condition and the heat equation. A more detailed discussion on the temperature history during tempering is given in [15,16].

2.1. Viscoelasticity

For linear viscoelastic materials, the Boltzmann superposition principle holds and the constitutive law can be formulated by a convolution integral. Using index notation and assuming zero initial strain, the constitutive equations can be written as

$$\sigma_{ij}(t) = 2 \int_0^t G(t-t') \frac{de_{ij}(t')}{dt'} dt' + \delta_{ij} \int_0^t K(t-t') \frac{d\varepsilon_{ii}(t')}{dt'} dt' \quad (2)$$

where σ_{ij} is the stress tensor, t is the time, t' is a running parameter for the time, ε_{ii} is the trace of the strain tensor, e_{ij} is the deviatoric strains, $G(t)$ and $K(t)$ are relaxation functions representing the time dependent shear and bulk modulus, respectively. The first term of the right hand side of (2) represents the deviatoric stresses, s_{ij} , while the second term represents to the hydrostatic stress, σ_{kk} .

A simple approach to include the temperature dependence is by changing the time-scale associated with the relaxation functions. Such behaviour is often referred to as a thermorheological simple (TS) [9] and it has been shown experimentally that glass is well represented by such a behaviour [8].

Utilizing the TS property, the relaxation function obtained at one temperature can be transformed to be valid for an arbitrary temperature by substituting the real time, t , with a scaled time,³ ξ . The scaling factor is temperature dependent and is most often referred to as the shift function,⁴ $\phi(T)$. The scaled time, ξ , for varying temperatures is found by integrating the shift-function, $\phi(T)$, over time

³ Often the term *reduced time* is used for ξ . This might be misleading since the theory covers both contraction and extension of the time scale.

⁴ The name "Shift function" refers to the derivation using a logarithmic time, where the scaling of linear time is represented by a shift.

$$\xi = \int_0^t \phi(T(t')) dt' \quad (3)$$

The temperature for which $\phi(T) = 1$ is referred to as the base temperature, T_B , indicating that $\phi(T_B) \equiv 1$. For most materials, the viscosity increases with decreasing temperature, corresponding to an extension of the time scale ($\phi(T) > 1$).

The shift-function relates the viscosity, η , at the base temperature, T_B , to the viscosity at the present temperature through a scaling in time

$$\eta(T_B)t = \eta(T)\xi \iff \xi = \frac{\eta(T_B)}{\eta(T)}t \Rightarrow \phi(T) = \frac{\eta(T_B)}{\eta(T)} \quad (4)$$

Several empirical shift functions have been proposed in order to fit the behavior of various materials, however, by assuming the behavior of a newtonian fluid, a shift function can be derived. The temperature variation of the viscosity follows a law of the Arrhenius type, see e.g. [17] and the shift function derived from the above assumptions can be written as

$$\ln \phi(T) = \ln \left(\frac{\eta(T_B)}{\eta(T)} \right) = \frac{H}{R_g} \left(\frac{1}{T_B} - \frac{1}{T} \right) \quad (5)$$

where H is the activation energy (627.8 kJ/mol for soda-lime glass [18]) and R_g is the universal gas constant (8.31 J/mol K).

2.2. Structural relaxation model

It has been shown that the rate of cooling (or heating) has an effect on certain properties such as viscosity and density [18]. This effect is attributed to the structural arrangement of the atoms (long range order) and it has turned out that the structure dependent density change is, by far, the most important regarding the residual stresses [13]. Therefore, only the change in density is considered here. Such relaxation is referred to as the volume relaxation due to mass conservation.

Fig. 2 sketches the development of the volume as a function of the temperature for different cooling rates. When the glass is cooled from above its melting temperature, T_m , it might crystallize when reaching T_m following Curve c in the figure, however, the rate of crystallization in silica glasses is very low and crystallization is unlikely to occur even for relatively slow cooling rates [19].

It is seen that for a relatively high cooling rate (Curve a), the density in the solid state becomes smaller (higher volume) than for a relatively lower cooling rate (Curve b). The dashed part on the curves indicate the glass transition range.

The phenomenon of structural relaxation was first treated by Tool [12] who introduced the fictive temperature, T_f , as a measure of the degree of non-equilibrated glass. The fictive temperature for a glass can be interpreted as the temperature where the extension

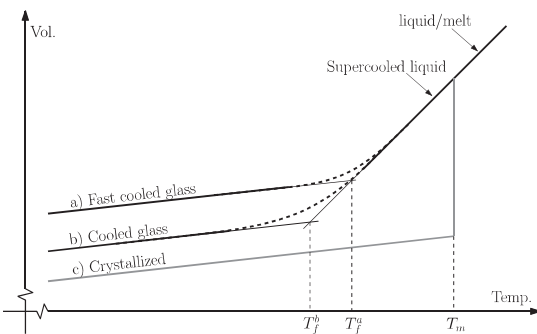


Fig. 2. Variation of volume with temperature for different cooling rates. Curve c represents the crystalline state with an abrupt change in volume when the melting temperature, T_m , is passed.

lines of the solid state and the liquid state intersect [20]. The fictive temperatures for a glass following Curves a and b in Fig. 2, respectively are denoted T_f^a and T_f^b as indicated in the figure.

In 1971 Narayanaswamy [11] proposed a mathematical formulation to be used in conjunction with the viscoelastic tempering model described in [10]. The structural model is capable of describing the property changes for different cooling rates, considerably improving the model based on viscoelasticity alone [13].

The fictive temperature for a specific property is found from the corresponding response function, $M(t)$, which is obtained experimentally. The equation for determining the fictive temperature from the response function is, see [11]:

$$T_f(t) = T(t) - \int_0^t M(\xi(t) - \xi'(t)) \frac{\partial T(t')}{\partial t'} dt' \quad (6)$$

where the scaled time is given by (3) using a shift function dependent on the fictive temperature, given by:

$$\ln(\phi_v(T, T_f)) = \frac{H}{R_g} \left(\frac{1}{T_B} - \frac{x}{T} - \frac{1-x}{T_f} \right) \quad (7)$$

with

$$H = H_g + H_s, \quad x = \frac{H_g}{H} \quad x \in [0; 1] \quad (8)$$

where H_g and H_s are the activation energies associated with temperature and structure (long range order), respectively and x is a factor controlling the relative influence of H_g and H_s .

When the fictive temperature is found from (6), the property associated with it can be derived. As stated before, only the volume relaxation is considered and due to the isotropy of the material this is accounted for by a change of the thermal strains. The thermal strains can now be found by the following relation

$$\Delta \epsilon_{ij}^{th} = \delta_{ij} \Delta \epsilon_{th} = \delta_{ij} (\alpha_g \Delta T + (\alpha_l - \alpha_g) \Delta T_f) \quad (9)$$

where α_l and α_g are the isotropic thermal expansion coefficients for the liquid and solid state, respectively.

When the temperature is high enough for the material to be in the liquid state the fictive temperature equals the real temperature, $T_f = T$, and the solid expansion coefficient, α_g cancels out in (9). During the transition, the fictive temperature is lacking behind the real temperature, $T < T_f$ (for cooling) and the expansion coefficient changes. When the temperature is low enough for the material to be solid, the fictive temperature is constant, $\Delta T_f = 0$, and the last term, including the liquid expansion coefficient α_l , vanishes.

3. Implementation

This section provides an implementation of the model described above, into a material routine for a finite element program. First the temperature independent linear viscoelastic model is treated, then it is extended to include the TS behavior, and finally, the structural volume relaxation is included. The algorithms are all well-known from literature such as [21–25].

3.1. Linear viscoelasticity

In general, an integration of the load history is needed in order to evaluate (2), however, such time and memory consuming operations can be avoided if the scaling of the relaxation functions is independent of the time considered, see e.g. [23]. This condition can be written as:

$$\frac{R(t + \Delta t)}{R(t)} = f(\Delta t) \quad (10)$$

where $f(\Delta t)$ represents an arbitrary function, independent of the total time, t . This condition is satisfied for series of exponential func-

tions which, therefore, with great advantage can be used for describing the viscoelastic behaviour of the shear and bulk relaxation moduli, $G(t)$ and $K(t)$, respectively.

$$\begin{aligned} G(t) &= \sum_{n=1}^{N_G} g_n \exp\left(-\frac{t}{\lambda_n^g}\right) \\ K(t) &= \sum_{n=1}^{N_K} k_n \exp\left(-\frac{t}{\lambda_n^k}\right) \end{aligned} \quad (11)$$

In Fig. 3, a mechanical interpretation of $G(t)$ in (11) is shown. The mechanical model represents the *generalized Maxwell* material constructed by N_G single *Maxwell* elements in parallel. Each Maxwell element consists of a spring stiffness, g_n , and a dashpot with the relaxation time λ_n^g in a sequence. The exponential series might also include a constant term for describing the deferred moduli, and are often referred to as Prony series. However, here the deferred modulus will be represented by an extra exponential term with a large relaxation time, $\lambda \gg t$.

It should be noted that the strains in each branch of the generalized Maxwell element are equal, (12), and that the total stress equals the sum of the stress in each branch, (13).

$$e_{ij}^{(1)} = e_{ij}^{(2)} = \dots = e_{ij}^{(N_G)} \quad (12)$$

$$s_{ij} = \sum_{n=1}^{N_G} s_{ij}^{(n)} \quad (13)$$

An analogous interpretation can be made for $K(t)$ and the hydrostatic stress, σ_{ii} .

In Fig. 4 a step in time from t to $t + \Delta t$ is shown on the horizontal axis and the stress associated with this increment is shown on the vertical axis. The stress increment is divided into two parts: one considering the viscoelastic response to the actual strain increment, $\Delta\tilde{\sigma}_{ij}$, and another considering the relaxation of the current total stress state $\Delta\tilde{\sigma}_{ij}$, shown as Curves b and d, respectively. Using (2) the viscoelastic response to the applied strain, $\Delta\tilde{\sigma}_{ij}$, can be written as:

$$\begin{aligned} \Delta\tilde{\sigma}_{ij} &= 2 \int_t^{t+\Delta t} G(t + \Delta t - t') \frac{\partial e_{ij}(t')}{\partial t'} dt' \\ &+ \delta_{ij} \int_t^{t+\Delta t} K(t + \Delta t - t') \frac{\partial e_{ii}(t')}{\partial t'} dt' \end{aligned} \quad (14)$$

By assuming a linear strain variation in each time step and evaluating the integral of the exponential series analytically Eq. (14) may, when writing the deviatoric and hydrostatic part separately, be written as

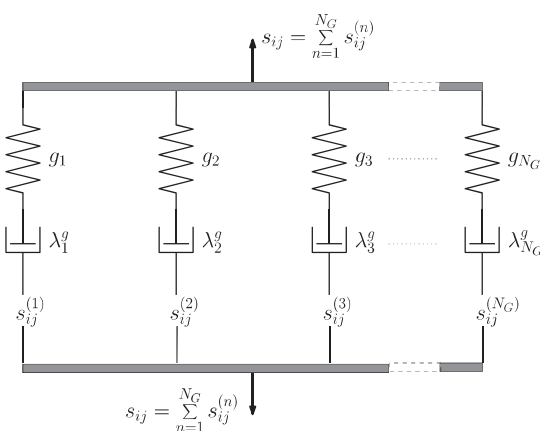


Fig. 3. Generalized Maxwell element with N_G branches for the deviatoric stresses, s_{ij} .

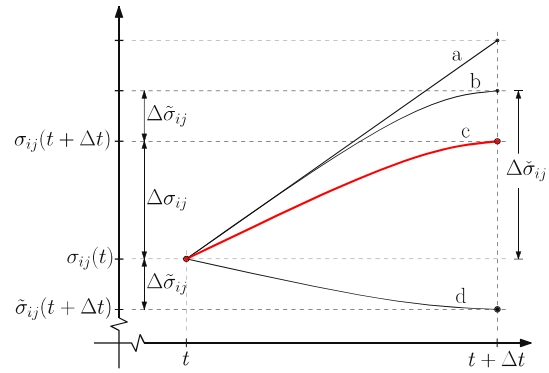


Fig. 4. Incremental formulation for the viscoelastic stress response. The increment has been divided into two parts; the viscoelastic increment and the decay of the current stress state.

$$\Delta\tilde{s}_{ij}^{(n)} = 2g_n \frac{\Delta e_{ij}}{\Delta t} \lambda_n^g \left(1 - \exp\left(-\frac{\Delta t}{\lambda_n^g}\right) \right) \quad (15a)$$

$$\Delta\tilde{\sigma}_{ii}^{(n)} = k_n \frac{\Delta e_{ii}}{\Delta t} \lambda_n^k \left(1 - \exp\left(-\frac{\Delta t}{\lambda_n^k}\right) \right) \quad (15b)$$

for each term in the exponential series in (11).

The stress relaxation of the current stress state, $\Delta\tilde{\sigma}_{ij}(t)$, is found by scaling, using the relaxation function. This scaling eliminates the need for an integration of the full load history and complies with (10) if it is done for each term in the exponential series. The new stress state at $t + \Delta t$ is denoted $\tilde{\sigma}_{ij}(t + \Delta t)$ which, in terms of deviatoric and hydrostatic stresses, can be written as

$$\tilde{s}_{ij}^{(n)}(t + \Delta t) = s_{ij}^{(n)}(t) \exp\left(-\frac{\Delta t}{\lambda_n^g}\right) \quad (16a)$$

$$\tilde{\sigma}_{ii}^{(n)}(t + \Delta t) = \sigma_{ii}^{(n)}(t) \exp\left(-\frac{\Delta t}{\lambda_n^k}\right) \quad (16b)$$

Hence, only the total stress for each term in (11) is needed from the previous time step, not the complete history.

The total stress increment for each branch in the generalized Maxwell material can now be calculated by adding (15) and (16).

$$s_{ij}^{(n)}(t + \Delta t) = \Delta\tilde{s}_{ij}^{(n)} + \tilde{s}_{ij}^{(n)}(t + \Delta t) \quad (17a)$$

$$\sigma_{ii}^{(n)}(t + \Delta t) = \Delta\tilde{\sigma}_{ii}^{(n)} + \tilde{\sigma}_{ii}^{(n)}(t + \Delta t) \quad (17b)$$

The total stress tensor, σ_{ij} , is found by summing over all branches.

$$\sigma_{ij}(t + \Delta t) = \sum_{n=1}^{N_G} s_{ij}^{(n)}(t + \Delta t) + \delta_{ij} \sum_{n=1}^{N_K} \sigma_{ii}^{(n)}(t + \Delta t) \quad (18)$$

The total stress is represented as Curve c in Fig. 4.

3.2. Thermorheological simplicity

In order to implement the TS material behavior the real time increment, Δt , has to be substituted with the scaled time increment, $\Delta\xi$. Rewriting (3) to an incremental form and using the trapezoidal integration rule (assuming linear temperature variation in the step), the scaled time step may be written as

$$\Delta\xi = \int_t^{t+\Delta t} \phi dt' \approx \frac{\Delta t}{2} (\phi(T + \Delta T) - \phi(T)) \quad (19)$$

where $\phi(T)$ is found from Eq. (5).

The value of the scaled time may vary with several orders of magnitude depending on the temperature, which might cause numerical problems when the material behaves almost like a linear elastic material and the scaled time step becomes small

$(\Delta\xi \rightarrow 0)$. A remedy for this problem is to use a Taylor expansion for the critical part of (15) when $\Delta\xi \rightarrow 0$

$$\frac{\lambda}{\Delta\xi} \left[1 - \exp \left(-\frac{\Delta\xi}{\lambda} \right) \right] = \frac{\lambda}{\Delta\xi} \left(1 - \sum_{k=0}^{\infty} \frac{1}{k!} \left(-\frac{\Delta\xi}{\lambda} \right)^k \right) \quad (20)$$

An investigation reveals that using the first three terms in the Taylor expansion for $\Delta\xi < 10^{-7}$ causes relative errors less than 10^{-10} .

For high temperatures a considerable decay of the stresses occurs and convergence will be slow if the linear elastic material tangent stiffness is used. By updating the material tangent stiffness matrix, D_T , using (15) the convergency rate can be improved. Curves a and b in Fig. 4 represent the linear elastic step and the viscoelastic step, respectively. The viscoelastic material tangent stiffness matrix can be written as

$$\mathbf{D}_T = \begin{bmatrix} B + 4A & B - 2A & B - 2A & 0 & 0 & 0 \\ B - 2A & B + 4A & B - 2A & 0 & 0 & 0 \\ B - 2A & B - 2A & B + 4A & 0 & 0 & 0 \\ 0 & 0 & 0 & 3A & 0 & 0 \\ 0 & 0 & 0 & 0 & 3A & 0 \\ 0 & 0 & 0 & 0 & 0 & 3A \end{bmatrix} \quad (21)$$

where

$$A = \frac{1}{3} \sum_{n=1}^{N_G} g_n \frac{\lambda_n^g}{\Delta t} \left(1 - e^{-\frac{\Delta t}{\lambda_n^g}} \right), \quad B = \sum_{n=1}^{N_K} k_n \frac{\lambda_n^g}{\Delta t} \left(1 - e^{-\frac{\Delta t}{\lambda_n^g}} \right) \quad (22)$$

3.3. Structural volume relaxation

The structural relaxation is inherently non-linear as seen from (6) and (7), however, by describing the response function $M(\xi)$ by an exponential series, an efficient and stable algorithm as proposed by Markovsky and Soules [26] may be utilized for solving the equations, and thereby determining the fictive temperature T_f . The exponential series reads:

$$M(\xi) = \sum_{n=1}^{N_M} m_n \exp \left(-\frac{\xi(T, T_f)}{\lambda_n^m} \right), \quad \sum_{n=1}^{N_M} m_n = 1 \quad (23)$$

where ξ depends on both T and T_f , and can be found from (7). In the algorithm for obtaining T_f from (6), a “partial fictive temperature” $T_f^{(n)}$ which is linked to the n'te term in the response function (23), is calculated from

$$T_f^{(n)}(t) = \frac{\lambda_n^m T_f^{(n)}(t - \Delta t) + T(t) \Delta t \phi_v}{\lambda_n^m + \Delta t \phi_v} \quad (24)$$

where

$$\phi_v = \exp \left[\frac{H}{Rg} \left(\frac{1}{T_B} - \frac{x}{T(t)} - \frac{1-x}{T_f(t - \Delta t)} \right) \right] \quad (25)$$

The fictive temperature at the current time, $T_f(t)$, is then given by the sum of the partial fictive temperatures weighted with m_n

$$T_f(t) = \sum_{n=1}^{N_M} m_n T_f^{(n)}(t) \quad (26)$$

The initial conditions for $T_f^{(n)}$ and T_f are:

$$T_f^{(n)}(0) = T(0), \quad T_f(0) = T(0) \quad (27)$$

It is seen that each partial fictive temperature, $T_f^{(n)}$, from the previous time step is needed together with the fictive temperature, T_f , from the previous time step.

The algorithm above can be shown to be stable for monotonic temperature changes [26].

The thermal strain increments, $\Delta\varepsilon_{ij}^{th}$, can now be found by the use of (9) and are subtracted from the normal strain increments originating from the mechanical boundary conditions, $\Delta\varepsilon_{ij}^{mech}$,

$$\Delta\varepsilon_{ij} = \Delta\varepsilon_{ij}^{mech} - \Delta\varepsilon_{ij}^{th} \quad (28)$$

From this strain increment tensor the deviatoric strain increment can be calculated as

$$\Delta e_{ij} = \Delta\varepsilon_{ij} - \frac{1}{3} \delta_{ij} \Delta e_{ii} \quad (29)$$

In order to summarize this section, an overview of the implementation of the model is given in Fig. 5. The parameters to the left of an arrow are needed in order to calculate the result provided to the right of the arrow. The numbers above the arrows refer to the relevant equations in the present paper.

FICTIVE TEMPERATURE

for $n=1$ to N_m **do**
 $\lambda_n^m, T_f^{(n)}(t - \Delta t), T(t), \Delta t,$ } $\xrightarrow{(24)}$
 $\phi_v(T(t), T_f(t - \Delta t))$
 $T_f^{(n)}(t)$
 $m_n, T_f^{(n)}(t) \xrightarrow{(26)} T_f(t)$
end for

STRAIN INCREMENTS

$\alpha_g, \alpha_l, \Delta T, \Delta T_f \xrightarrow{(9)} \Delta\varepsilon_{ij}^{th}$
 $\Delta\varepsilon_{ij}^{mech}, \Delta\varepsilon_{ij}^{th} \xrightarrow{(28)} \Delta\varepsilon_{ii}$
 $\Delta\varepsilon_{ij} \xrightarrow{(29)} \Delta e_{ij}$

SHIFTED TIME

$\Delta t, \phi(T(t), T(t + \Delta t)) \xrightarrow{(19)} \Delta\xi$

DEVIATORIC STRESSES

for $n=1$ to N_G **do**
 $g_n, \lambda_n^g, \Delta e_{ij}, \Delta\xi \xrightarrow{(15a)/(20)} \Delta s_{ij}^{(n)}$
 $\lambda_n^g, s_{ij}^{(n)}(t), \Delta\xi \xrightarrow{(16a)} \tilde{s}_{ij}^{(n)}(t + \Delta t)$
 $\tilde{s}_{ij}^{(n)}(t + \Delta t), \Delta s_{ij}^{(n)} \xrightarrow{(17a)} s_{ij}^{(n)}(t + \Delta t)$
end for

HYDROSTATIC STRESS

for $n=1$ to N_K **do**
 $k_n, \lambda_n^k, \Delta\varepsilon_{ii}, \Delta\xi \xrightarrow{(15b)/(20)} \Delta\check{\sigma}_{ii}^{(n)}$
 $\lambda_n^k, \sigma_{ii}^{(n)}(t), \Delta\xi \xrightarrow{(16b)} \check{\sigma}_{ii}^{(n)}(t + \Delta t)$
 $\check{\sigma}_{ii}^{(n)}(t + \Delta t), \Delta\check{\sigma}_{ii}^{(n)} \xrightarrow{(17b)} \sigma_{ii}^{(n)}(t + \Delta t)$
end for

TOTAL STRESSES

$s_{ij}^{(n)}(t + \Delta t), \sigma_{ii}^{(n)}(t + \Delta t) \xrightarrow{(18)} \sigma_{ij}(t + \Delta t)$

Fig. 5. Overview of the implementation of the tempering model.

4. Convergence, verification and application

The algorithm has been implemented as a material subroutine in the commercial finite element program Abaqus [27]. This section validates the model and investigates the discretization regarding time and geometry. Experimental validation of the tempering theory presented has been reported for a 1D model by [13] and a 3D model by Daudeville and Carre [14]. However, the present paper presents a comparison with experiments and a discussion of the deviations for different cooling rates which has not, to the knowledge of the authors, been reported before.

4.1. Comparison with analytical solution

In order to verify the thermorheologically simple part of the implementation, an analytical one-dimensional model for a prescribed load- and temperature history has been derived, see Appendix A. The relaxation modulus, the load and the temperature used in the analytical solution have been fitted to a numerical simulation of the tempering process at the surface, however, it should be emphasized that the solution does not reflect any physical process and that the model only describes a single material point. The numerical solution is therefore independent of the number of elements used, however, it provides a convenient way to test the specific part of the implementation.

Fig. 6 shows the analytical solution together with the solutions obtained from the implementation presented in Section 3 (without structural relaxation). From the figure it is seen that the simulation follows the analytical solution.

4.2. Comparison with experimental results

Experimental results for the tempering process are rarely reported in the literature, however [28] presents an experimental investigation of the mid-plane stress for varying initial temperatures, T_{init} and forced convection constants, h .

In Fig. 7 the model is compared with the test results. It is seen that the model captures the observed trend from the experiments quite well. It is worth noting that for $h = 222 \text{ W/m}^2 \text{ K}$ there is a good correlation between the model and the experimental results. This value of h corresponds to what is needed for producing commercially tempered glass according to [28].

The experiments conducted in [28] are of a relatively complex nature and uncertainties on e.g. the determination of h and the residual stresses are present. In order to see if the model can be fitted in a simple manner to more accurately represent the experimental observations, a fit using h as the only parameter is performed. This is motivated by assuming that there might be an error in the measurement of h which is a function of the air flow velocity (expressed by h itself). The fitted values of h are

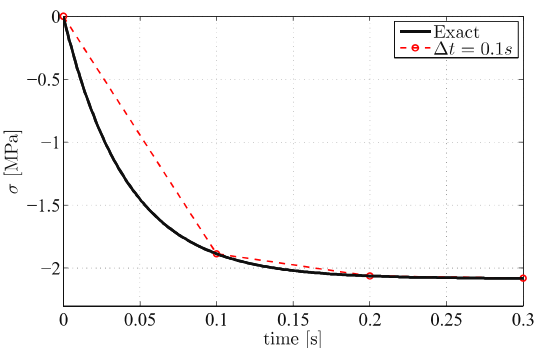


Fig. 6. The analytical solution along with a run using $\Delta t = 0.1 \text{ s}$. Parameters used for the analytical solution are found in Table A.1.

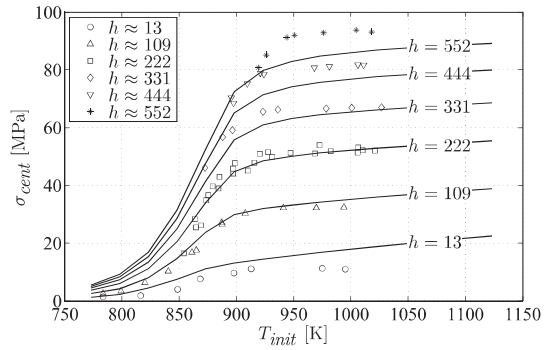


Fig. 7. Experimental validation of model for different forced convection constants, h , and initial temperatures, T_{init} . Experimental results are found in [28]. The forced convection constants have the unit of $\text{W}/(\text{m}^2 \text{ K})$.

denoted h_{fit} and the obtained correlation between h and h_{fit} is shown in Fig. 8.

Using the fitted values of h for the modeling and comparing with the experimental results, Fig. 9 is obtained.

It is seen that with such simple adjustment, the model is capable of reproducing the experimental results quite accurately even for relatively extreme cooling rates. This indicates that there might be uncertainties in the experimental work in [28] and these may be accounted for (by modifying h).

4.3. Convergence

The implementation presented previously can be used for simulating the state of residual stress in complex 3D geometries modeled using solid elements. In general the convergence is dependent on the problem simulated. However, in this section, a model representing the stress state through the thickness of a glass plate is used for investigating the convergence. However, the presented curves are in principle only valid for the specific parameters used here.

The plate considered is 19 mm thick and cooled symmetrically from both sides. The models described in this section consists of solid elements with proper boundary conditions, representing the large distance to the edges, (see [29]). Relevant model parameters can be found in Appendix B.

The development of stresses over time at the surface and in the center is shown in Fig. 10. It is seen that during the transition period the surface goes into tension. The maximum transient tensile surface stress is denoted $\sigma_{surf,max}$ as shown in the figure. When the plate has cooled to a uniform temperature in the solid state, the stresses will be constant and referred to as the steady state

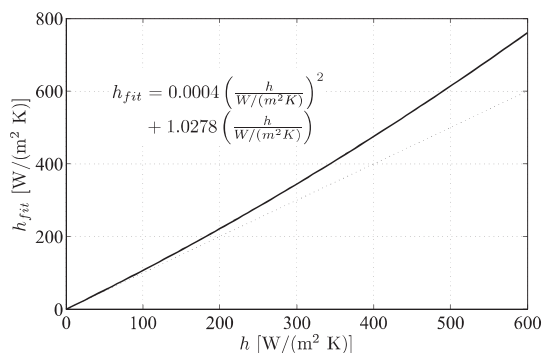


Fig. 8. Fitted values of the forced convection constant h_{fit} as a function of the originally used forced convection constant, h .

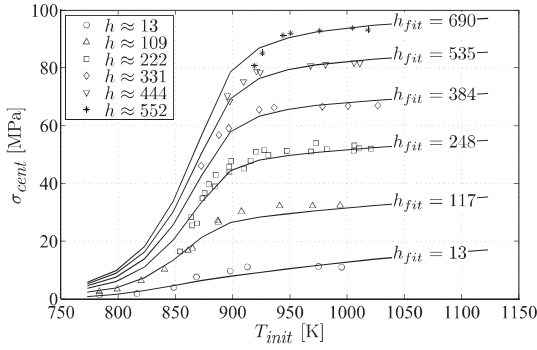


Fig. 9. Comparison with experiments [28] using the fitted values for the forced convection constant, h_{fit} . The forced convection constants have the unit of $\text{W}/(\text{m}^2 \text{K})$.

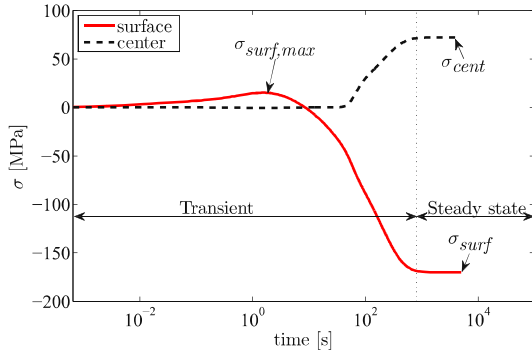


Fig. 10. Typical development of the surface and center stresses during the cooling process.

stresses, denoted σ_{cent} and σ_{surf} for the center and surface stresses, respectively, see Fig. 10.

These three stresses are considered for convergency throughout this investigation. The model is implemented in a material user-subroutine in Abaqus and 20-node coupled displacement-temperature continuum elements with quadratic displacement fields and linear temperature field have been applied. The results in this section are normalized using the most trustworthy solution, meaning the solution with most elements and/or smallest time-steps.

The curves in Fig. 11 show the convergence for perfectly cubic shaped solid elements, uniformly distributed. The cooling rate is controlled by the forced convection constant, h . A convergency analysis for three different values of h is performed and shown in Fig. 11. The value $h = 280.1 \text{ W/m}^2 \text{ K}$ is reported by Daudeville and Carre [14] for a 6 mm thick plate and must be considered quite high for a 19 mm plate, indicating a more severe cooling than required for obtaining a reasonable level of residual stress values.

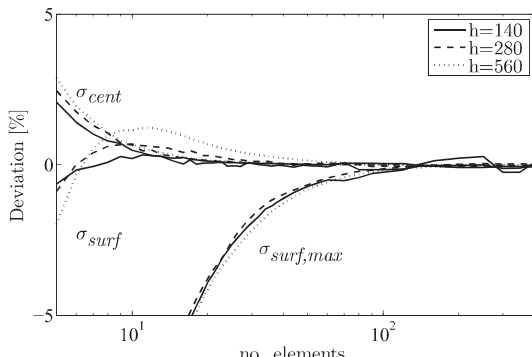


Fig. 11. Convergency for uniformly distributed 20-node hexahedron elements for different cooling rates.

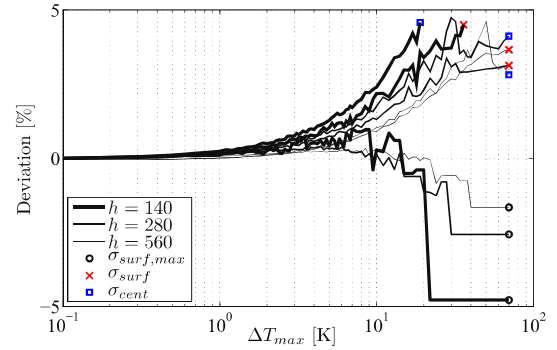


Fig. 12. Step size convergency, regulated using a maximum temperature change, ΔT_{max} , in the increment.

In Fig. 11 it is seen that for an increasing cooling rate; the deviation for σ_{surf} is slightly increased for an equal number of elements. It is furthermore seen that for the steady-state stresses, five elements through half the thickness provides a reasonable convergence, however, for the transient stress more than fifteen uniformly distributed elements are required for reaching convergence within 5%.

An investigation on the influence of the time step has been carried out. The step size was controlled by setting a limit to the maximum temperature change, ΔT_{max} , within an increment. From Fig. 12 it is seen that care should be taken when allowing for too large temperature changes in each step (large time steps).

In order to minimize the number of elements, an investigation on how the transient stresses converge towards the best solution (1200 elements) is shown in Fig. 11. From this figure it is seen that convergence is reached for the residual steady-state stresses (far from any edges) with quite few elements through the thickness. However, the transient surface tensile stresses require more elements for reaching convergence due to the more complex transient stress distribution.

By increasing the mesh density near the surface, convergence can be reached with fewer elements. For investigating this we define the bias factor as the ratio between the length of the center element and the length of the surface element in the direction along the surface normal.

These investigations revealed that the biased mesh had a major positive effect on the convergence of the transient stresses, a small effect on the steady state center stresses and an insignificant effect on the steady state surface stress. In Fig. 13 (only showing the transient stresses) it is seen that the convergence improve with higher bias ratio, however, since the steady state center stresses diverge for an increased bias ratio, an optimum exists.

As a result of the diverging tensile stresses, the curves in the figure do not approach the solution obtained for 1200 uniformly dis-

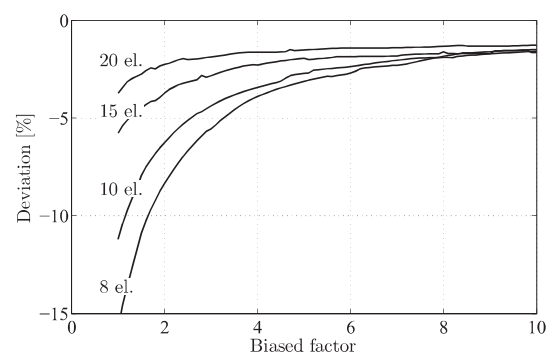


Fig. 13. Biased element convergency for the transient surface stress, $\sigma_{surf,max}$.

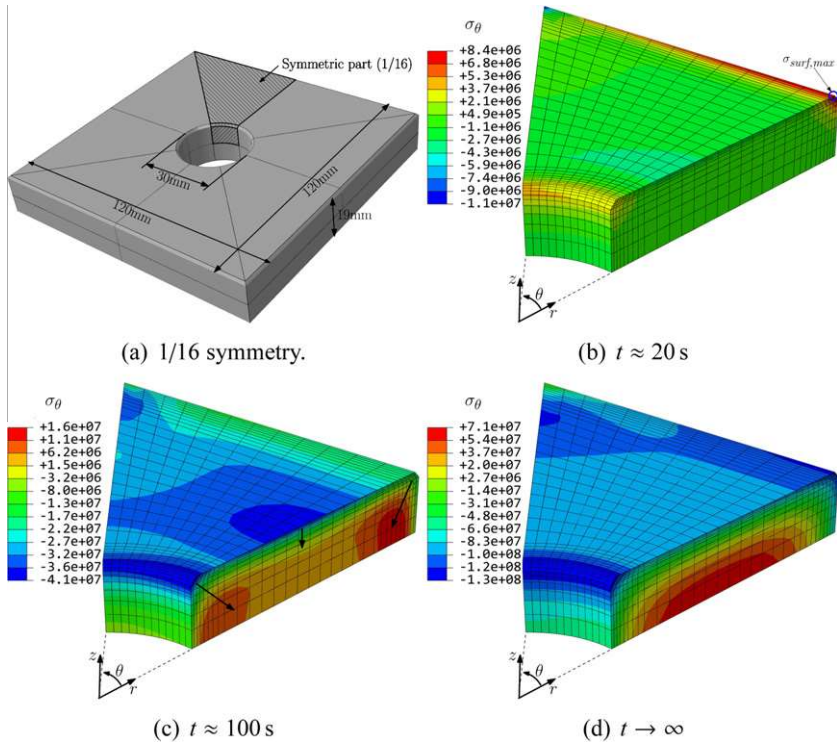


Fig. 14. The development of (tangential) stresses, σ_θ during tempering.

tributed elements. A recommended bias ratio for this type of problem would be between 4 and 8, with the element size decreasing towards the surface. However, it should be emphasized that the stress state at corners and edges is more complex and requires more elements.

4.4. 3D residual stress field – example

The possible applications for the model described and validated in the preceding are numerous. This example shows the evolution of tempering stresses in a square glass plate with a centrally located hole (see Fig. 14a), during the process. In Fig. 14, 1/16 of the geometry is shown at three different times. In this case the maximum transient stress is found at the edge after approximately 20 s of cooling (Fig. 14b). After approximately 100 s the surface is in compression and the compression zones are seen to expand, increasing the tensile stresses in the interior (Fig. 14c). Finally the temperature is uniformly distributed and the residual (steady-state) stresses are shown in Fig. 14d. Due to the variation in the residual stresses, a spatial dependency of the apparent strength is a consequence. Stresses far away from the edges approach a planar hydrostatic stress state corresponding to the results found in the previous section.

For plates with holes, the largest compressive stresses are typically found in the surface of the hole near the surface of the plate and most far away from the corner. A parametric investigation of the residual stresses at holes for different geometries may be found in [30].

5. Conclusion

The theory and implementation of a model predicting the evolution of 3D stress state during the glass tempering process is developed. The model is based on thermorheological simplicity and structural relaxation. The thermorheologically simplicity re-

lates the decay of stresses to the temperature history, while the structural relaxation relates the density change to the history of the cooling rate. The theory and implementation of these models is comprehensively described in order to enable the reader to easily understand and implement such model in own code.

The implemented model is capable of predicting transient stresses as well as steady-state stresses for complex geometries and thereby provides a strong tool for optimization of the tempering process as well as estimating the steady-state residual stresses in tempered glass in order to evaluate the spatially dependent apparent strength. An analytical expression for testing the thermorheologically part of the model have been derived and used for verifying that part of the model.

The model has also been validated against experimental data showing that for commonly used convection constants for tempered glass, the model is quite accurate. For high or low cooling rates the model deviates more from the experimental results, however, it is shown that this can be accounted for by adjusting a single parameter, namely the forced convection constant h .

Convergence analyses have been performed on a model representing a symmetrically cooled glass plate far from any edge. It was found that the convergence depends on the cooling rate, however, the dependency is weak for realistic values of the cooling rate quantified by the forced convection constant h .

Finally, an example showing the stress state at three different stages for a square glass plate with a centrally located hole is given.

Appendix A. Analytical solution

The solid considered has a known temperature history, independent of the spatial coordinates, x_i , and without any thermal contraction.

$$T(x_i, t) = T(t) = \frac{c}{\ln(at + b)} \quad (\text{A.1})$$

Table A.1

Constants used for the analytical solution presented in Fig. 6.

$a = 0.2957 \text{ 1/s}$	$b = 6.937$
$c = 1.676 \times 10^3 \text{ K}$	$H = 22.380 \times 10^3 \text{ K}$
$T_B = 779.9 \text{ K}$	$k = -1.231 \times 10^8 \text{ 1/s}$
$E_0 = 70 \times 10^9 \text{ Pa}$	$\lambda = 0.7012 \text{ s}$

where t is the time and a, b, c are constants to be defined. Using the shift function defined in (5), and substituting the temperature relation from (A.1) we find

$$\ln(\phi(T)) = H \left(\frac{1}{T_B} - \frac{\ln(at + b)}{c} \right) \quad (\text{A.2})$$

where T_B and H are constants to be defined.

The relaxation modulus for uniaxial load is described by a single exponential term:

$$E(t) = E_0 e^{-\frac{t}{\lambda}} \quad (\text{A.3})$$

where E_0 and λ are constants to be defined.

The material is exposed uniaxially to a prescribed strain, which is a known function of time.

$$\frac{d\varepsilon(t)}{dt} = \begin{cases} k(at + b)^{(-\frac{H}{c})} & \text{for } t \geq 0 \\ 0 & \text{for } t < 0 \end{cases} \quad (\text{A.4})$$

where k is the only constant to be defined, since the rest are known from the previous equations.

Due to the uniaxial load and the independency of the spatial coordinates the convolution integral can be written as

$$\sigma(t) = \int_0^t E(\xi - \xi') \frac{d\varepsilon(t')}{dt'} dt' \quad (\text{A.5})$$

where ξ and ξ' are defined by (3) by using t and t' as the upper integration bound, respectively. The integration of (A.5) can be done analytically and yields.

$$A_1 \sigma(t) = \exp \left[A_5 b T_B (at + b)^{A_3} - A_5 T_B b^{A_3+1} + A_5 t a T_B (at + b)^{A_3} - A_2 H a \lambda \right] + A_4 \quad (\text{A.6})$$

where

$$A_1 = \frac{-1}{\lambda E_0 k} \exp \left(\frac{H(H - 2c)}{T_B(H - c)} \right)$$

$$A_2 = \frac{c}{a\lambda T_B(H - c)}$$

$$A_3 = -\frac{H}{c}$$

$$A_4 = -\exp \left(\frac{-Hc}{T_B(H - c)} \right)$$

$$A_5 = A_2 \exp \left(\frac{H}{T_B} \right)$$

Appendix B. Modeling parameters

The thermal conductivity, λ_{th} , and the specific heat, C , for soda-lime-silica glass as function of the temperature, T , is given in [14]:

$$\lambda_{th} = 0.741 \text{ W/m K} + T \cdot 8.58e - 4 \text{ W/m K}^2 \quad (\text{B.1})$$

$$C = \begin{cases} 1433 + 6.5 \times 10^{-3} T & T \geq 850 \text{ K} \\ 893 + 0.4T - 18 \times 10^{-8} T^{-2} & T < 850 \text{ K} \end{cases}$$

The unit of C is J kg K if the temperature is given in Kelvin. All other parameters used for the model can be found in Tables B.2–B.4.

Table B.2

Material data for the generalized Maxwell material. The data is derived from [14].

n	$g_n \text{ (GPa)}$	$\lambda_n^g \text{ (s)}$	$k_n \text{ (GPa)}$	$\lambda_n^k \text{ (s)}$
1	1.585	6.658×10^{-5}	0.7588	5.009×10^{-5}
2	2.354	1.197×10^{-3}	0.7650	9.945×10^{-4}
3	3.486	1.514×10^{-2}	0.9806	2.022×10^{-3}
4	6.558	1.672×10^{-1}	7.301	1.925×10^{-2}
5	8.205	7.497×10^{-1}	13.470	1.199×10^{-1}
6	6.498	3.292	10.900	2.033
7			7.500	∞
sum	28.686		41.670	

Table B.3

Material data for the response function (23) for the structural volume relaxation. The data is derived from [14].

n	$m_n \text{ (-)}$	$\lambda_n^m \text{ (s)}$
1	5.523×10^{-2}	5.965×10^{-4}
2	8.205×10^{-2}	1.077×10^{-2}
3	1.215×10^{-1}	1.362×10^{-1}
4	2.286×10^{-1}	1.505×10^{-1}
5	2.860×10^{-1}	6.747
6	2.265×10^{-1}	29.630

Table B.4

Modeling parameters used.

Parameter	Value	Refs.
Plate thickness	19 mm	–
Activation energy (total), H	457.05 kJ/mol	[14]
structural/total ratio, x	0.5	[18]
Ideal Gas constant, R_g	8.31 J/mol	–
Base temperature, T_B	869 K	[14]
Solid thermal expansion, α_s	$9.10 \times 10^{-6} \text{ K}^{-1}$	[14]
Liquid thermal expansion, α_l	$25.10 \times 10^{-6} \text{ K}^{-1}$	[14]
Density, ρ	2500 kg/m ³	[3]
Initial Temperature, T_{init}	923.15 K	–
Ambient Temperature, T_∞	293.15 K	–
Forced convection constant, h	280.1 W/m ² K	[14]

References

- [1] Nielsen JH, Olesen JF, Stang H. The fracture process of tempered soda-lime-silica glass. Experimental Mechanics 2009;49(6):855.
- [2] Barsom J. Fracture of tempered glass. Journal of the American Ceramic Society 1968;51(2):75–8.
- [3] Haldimann M, Luible M. Overend, Structural Use of Glass, IABSE, 2008.
- [4] EN12150-1, Glass in building – thermally toughened soda lime silicate safety glass – Part1: Definition and descriptions (11 2004).
- [5] O. Narayanaswamy, Evolution of glass tempering models, in: Glass Processing Days, 2001.
- [6] Adams L, Williamson E. The annealing of glass. Journal of the Franklin Institute 1920;190:597–632.
- [7] G. Bartenev, The phenomenon of the hardening of glass, Journal of Technical Physics 18 (in Russian).
- [8] Kurkjian C. Relaxation of torsional stress in transformation range of soda-lime-silica glass. Physics and Chemistry of Glasses 1963;4(4):128–36.
- [9] Schwarzl F, Staverman A. Time-temperature dependence of linear viscoelastic behavior. Journal of Applied Physics 1952;23(8):838–43.
- [10] Lee E, Rogers T, Woo T. Residual stresses in a glass plate cooled symmetrically from both surfaces. Journal of the American Ceramic Society 1965;48(9).
- [11] Narayanaswamy O. A model of structural relaxation in glass. Journal of the American Ceramic Society 1971;54(10):491–8.
- [12] Tool A. Relation between inelastic deformability and thermal expansion of glass in its annealing range. Journal of the American Ceramic Society 1946;29(9):240–53.
- [13] Narayanaswamy O. Stress and structural relaxation in tempering glass. Journal of the American Ceramic Society 1978;61(3–4):146–52.
- [14] Daudeville L, Carre H. Thermal tempering simulation of glass plates: inner and edge residual stresses. Journal of Thermal Stresses 1998;21(6):667–89.
- [15] Laufs W, Sedlacek G. Stress distribution in thermally tempered glass panes near the edges, corners and holes. Part 1: temperature distributions during the

- tempering process of glass panes. *Glass Science and Technology: Glastechische Berichte* 1999;72(1):7–14.
- [16] T. Bernard, R. Gy, L. Daudeville, Finite element computation of transient and residual stresses near holes in tempered glass plates, in: 19th International Congress on Glass, 2001, pp. 445–446.
 - [17] Laidler KJ, Meiser JH. *Physical Chemistry*. third ed. Houghton Mifflin; 1999.
 - [18] Uhlmann DR, Kreidl NJ. *Glass Science and Technology 5: Elasticity and Strength in Glasses*. Academic Press; 1980.
 - [19] Rao KJ. *Structural Chemistry of Glasses*. Elsevier; 2002.
 - [20] Shelby J. *Introduction to Glass Science and Technology*. second ed. The Royal Society of Chemistry; 2005.
 - [21] Snyder MD, Bathe K-J. A solution procedure for thermo-elastic-plastic and creep problems. *Nuclear Engineering and Design* 1981;64(1):49–80.
 - [22] Simo JC, Hughes TJR. *Computational Inelasticity*. Springer Science; 1998.
 - [23] Zienkiewicz O, Taylor R. *The Finite Element Method – Solid Mechanics*. fifth ed. Butterworth-Heinemann; 2000. vol. 2, 459 p., English.
 - [24] Kojic M, Bathe KJ. *Inelastic Analysis of Solids and Structures*. Springer; 2005.
 - [25] Ibrahimbegovic A. *Nonlinear Solid Mechanics*. Springer Science; 2009.
 - [26] Markovsky A, Soules T. An efficient and stable algorithm for calculating fictive temperatures. *Journal of the American Ceramic Society* 1984;67(4):C56–7.
 - [27] Abaqus User Subroutines Reference Manual (v.6.7), 2007.
 - [28] R. Gardon, The tempering of flat glass by forced convection, in: Proc. Int. Congr. Glastt, 7th, Institut National du Verre, Charleroi, Belgique, 1965, p. Paper No. 79.
 - [29] J.H. Nielsen, Tempered glass – bolted connections and related problems, Ph.D. Thesis, Technical University of Denmark, Dept. of Civil Eng., 2010.
 - [30] J.H. Nielsen, J.F. Olesen, P.N. Poulsen, H. Stang, Simulation of residual stresses at holes in tempered glass – a parametric study. *Materials and Structures* (2009), doi:10.1617/s11527-009-9558-z.